Journal of Materials Chemistry A

PAPER

View Article Online
View Journal | View Issue



Cite this: J. Mater. Chem. A, 2014, 2, 19526

# Nano $La_{0.6}Ca_{0.4}Fe_{0.8}Ni_{0.2}O_{3-\delta}$ decorated porous doped ceria as a novel cobalt-free electrode for "symmetrical" solid oxide fuel cells

Guangming Yang,[a] Chao Su,*[b] Yubo Chen,[a] Moses O. Tadé[b] and Zongping Shao*[ab]

Received 8th July 2014
Accepted 4th October 2014

DOI: 10.1039/c4ta03485f

www.rsc.org/MaterialsA

Here we report that the nano $La_{0.6}Ca_{0.4}Fe_{0.8}Ni_{0.2}O_{3-\delta}$ (LCFN) decorated $Sm_{0.2}Ce_{0.8}O_{1.9}$ (SDC) composite oxide, prepared by the solution infiltration method, could function well as a cobalt-free electrode material for "symmetrical" solid oxide fuel cells (SOFCs). The structure, morphology, thermal expansion, oxygen reduction reaction activity and catalytic activity for methane oxidation of the as-prepared LCFN-infiltrated SDC electrode was investigated systematically. Under a reducing atmosphere, the partial segregation of metallic nickel from the LCFN perovskite lattice was demonstrated by SEM and STEM-EDX, and the XRD results suggested that the perovskite structure of LCFN still survived. Consequently, the good anode performance was expected due to the high catalytic activity of LCFN for methane oxidation and the excellent electrocatalytic activity of nano nickel for the methane reforming and electro-oxidation of hydrogen. In an air atmosphere, an area specific resistance as low as 0.12 Ω $cm^2$ was achieved at 600 °C. The SDC electrolyte supported "symmetrical" SOFC with the LCFN-infiltrated SDC electrode was then fabricated and tested, which delivered attractive peak power densities of 510 and 350 mW $cm^{-2}$ at 800 °C, operating on hydrogen and $CH_4$–$O_2$ fuels, respectively.

## Introduction

Fuel cells are one kind of electrochemical energy conversion devices that outperform traditional power generation devices based on combustion technology, in terms of efficiency, emission and noise reduction.[1,2] There are several types of fuel cells, which can be categorized based on the conducting species of the electrolyte, operating temperatures or fuels. Among them, solid oxide fuel cells (SOFCs) are of particular interest for their outstanding energy efficiency, fuel flexibility and high quality of exhaust heat, resulting from their high operation temperature ranging from 500 to 1000 °C.[3–5]

Although the exact reaction mechanism in a SOFC is fairly complicated and has not yet been fully understood, the simplified process may be described as follows. Molecular oxygen in the cathode atmosphere diffuses through the gas phase to adsorb on the surface of the porous cathode, where it is reduced to oxygen ions *via* a series of intermediate steps; then the oxygen ions are transported through the electrolyte to the anode where they react with fuel to produce the oxidation product with the simultaneous release of electrons, meanwhile the electrons move through the external circuit to the cathode to form a complete charge diffusion circle. Different materials are typically selected for the anode and cathode in a SOFC due to their different operation conditions, including oxygen partial pressure, reaction type and atmosphere composition. Up to now, the most applied anode materials in the SOFCs are nickel–electrolyte material cermets, while perovskite oxides are usually selected as the cathode materials,[6–9] therefore there are two different interfaces in a conventional SOFC, *i.e.*, the anode–electrolyte and cathode–electrolyte interfaces. The potential interfacial reaction and the mismatch in the thermal expansion coefficient (TEC) between the cell components could cause the performance degradation and even the failure of SOFCs. If the same material is used for both the anode and cathode, improved compatibility between cell components and reduced cell fabrication cost is expected because only one type of interface exists. According to the above considerations, symmetrical SOFCs with an identical material for both electrodes was proposed and investigated recently.[10–14]

To be a suitable electrode material for symmetrical SOFCs, it should meet the requirements of sufficient conductivity and thermo-mechanical stability under both the anode and cathode environments.[14,15] During the past, $LaCrO_3$-based perovskite oxides were mainly investigated, which can maintain a perovskite lattice structure over a wide range of oxygen partial pressures;[10,15,16] however, these materials usually show poor electrocatalytic activity for oxygen reduction reaction (ORR) and low conductivity at a reducing atmosphere (*i.e.*, anode atmosphere).

[a]State Key Laboratory of Materials-Oriented Chemical Engineering, College of Chemistry & Chemical Engineering, Nanjing Tech University, No. 5 Xin Mofan Road, Nanjing, 210009, China. E-mail: shaozp@yeah.net; Fax: +86 25 83172242; Tel: +86 25 83172256

[b]Department of Chemical Engineering, Curtin University, Perth, WA 6845, Australia. E-mail: chao.su@curtin.edu.au; Fax: +61 8 9266 2681; Tel: +61 8 9266 4702

As a result, a poor cell power output is usually obtained.[10,15,17] It suggests that the development of alternative materials is urgently needed in order to realize the practical use of symmetrical SOFCs. Recently, we proposed a new "symmetrical" SOFC, in which $K_2NiF_4$-type $La_2NiO_4$ was applied as the material for both electrodes.[18] Unlike most of the applied $LaCrO_3$-based electrodes, $La_2NiO_4$ was fully reduced to $La_2O_3$ and Ni under the anode atmosphere (thus, the cell was not actually symmetrical in composition under the practical operation conditions). The formed metallic Ni showed a high activity for fuel electro-oxidation. In addition, the electric conductivity of anode was improved significantly as compared to conventional oxide-based anodes. However, due to the large volume change associated with the phase change from $La_2NiO_4$ to $La_2O_3$ under the anode atmosphere, the mechanical integrity of the cell is still a big concern during the repeated redox cycles process.

In this study, we report a nano $La_{0.6}Ca_{0.4}Fe_{0.8}Ni_{0.2}O_{3-\delta}$ (LCFN) modified porous $Sm_{0.2}Ce_{0.8}O_{1.9}$ (SDC) composite as a novel cobalt-free electrode for "symmetrical" SOFCs, which was prepared by infiltrating LCFN into a porous SDC scaffold. Under the anode conditions, the LCFN in the infiltrated electrode was partially reduced with the segregation of nickel from the perovskite lattice that decorated the surface of the LCFN particles, but the perovskite phase structure was not destroyed, ensuring good redox cyclability. Moreover, the favorable activity of LCFN for methane oxidation and the good electrocatalytic activity of nano metallic Ni for methane reforming and electro-oxidation of $H_2$ resulted in the good performance of the LCFN modified SDC as an anode. As a result, an attractive cell performance was achieved with this new "symmetrical" SOFC. It thus provides a new promising electrode for symmetrical SOFCs, which may significantly promote the wide-spread application of this high temperature electrochemical device to build a lower-carbon sustainable society.

# Experimental

### Synthesis and fabrication

Single phase LCFN and SDC powders were synthesized *via* a combined EDTA–citric acid complexing method as reported elsewhere,[19] and their firing temperatures for phase formation were fixed at 1000 and 800 °C, respectively. The LCFN precursor solution for the infiltration was prepared in a similar way as reported in our previous work.[18] Briefly, stoichiometric amounts of $La(NO_3)_3\cdot 6H_2O$, $Ca(NO_3)_2\cdot 4H_2O$, $Fe(NO_3)_3\cdot 9H_2O$ and $Ni(NO_3)_3\cdot 6H_2O$ (analytical reagent) were mixed with deionized water to form a mixed solution with the nominal LCFN concentration of 0.6 mol $L^{-1}$, then glycine and ethanol were added as a complexing agent and a surfactant, respectively.

To fabricate cells in the symmetrical configuration for the cathodic performance evaluation, the as-synthesized SDC powder was firstly pressed into disk-shaped pellets with subsequent calcination at 1400 °C for 5 h, and then both surfaces of the sintered SDC electrolyte pellets were polished by a sand paper to a thickness of 0.3 mm. For the symmetrical cells with pure LCFN or a LCFN–SDC composite electrode (weight ratio of LCFN to SDC was 30 : 70) prepared by physical mixing method, the electrode, well dispersed in isopropyl alcohol, was symmetrically sprayed onto both sides of the as-prepared SDC electrolyte pellet, and finally calcined at 1000 °C for 2 h in air to obtain the cells. As for the fabrication of symmetrical cells with the infiltrated electrode, the details are described in our previous publication.[18] Briefly, a suspension comprised of SDC and soluble starch (pore former) was sprayed onto both surfaces of the SDC disk and subsequently fired at 1300 °C for 5 h in air to create the porous SDC scaffold, then the as-prepared LCFN precursor solution was infiltrated into the scaffold several times to reach the final loading of ~20 wt% during the overall infiltration. Finally, the symmetrical cells were calcined at 800 °C for 2 h in air to form the desired lattice structure.

To fabricate the electrolyte-supported "symmetrical" SOFC with the configuration of (anode) LCFN-infiltrated SDC|SDC|LCFN-infiltrated SDC (cathode) for the *I–V* and impedance tests, the effective electrode surface area of 0.48 $cm^2$ was adopted while the other preparation processes were the same as the previous section.

### Characterization

The phase structure of the prepared samples was determined by X-ray diffraction (XRD, D8 Advance Bruker) with filtered Cu-Kα radiation. The data was collected in a step-scan mode within a range of 20–90° with intervals of 0.02°. The more detailed structural information was conveyed by the Rietveld refinement of the XRD patterns with the GSAS-EXPGUI package. The microstructure of the LCFN-infiltrated electrodes was characterized by a field emission scanning electron microscope (FE-SEM, JEOL-S4800) and high resolution-transmission electron microscope (HR-TEM, JEOL JEM-2100). Bright-field scanning transmission electron microscopy (STEM) images were obtained using an FEI Tecnai G2 T20 electron microscope operating at 200 kV. The corresponding energy-dispersive X-ray (EDX) mappings were acquired using an FEI Tecnai G2 F30 S-TWIN field emission transmission electron microscope (FE-TEM) equipped with an EDX analyzer operating at 300 kV. The thermal expansion coefficient (TEC) data was collected using a Netzsch DIL 402C/3/G dilatometer in air from 200 to 1000 °C with a heating rate of 5 °C $min^{-1}$.

### Catalytic evaluation

A flow-through type fixed-bed quartz-tube reactor with an inner diameter of 8 mm was employed to assess the catalytic activity for methane oxidation of the fresh LCFN powder and the LCFN powder after the treatment in 10% $H_2$–Ar at 700 °C for 10 h. Approximately 0.2 g of catalyst particles with 40–60 mesh size were loaded in the middle of the reactor. The reactant, $CH_4$–$O_2$ gas mixture (2 : 1, volume ratio), was fed into the reactor with the flow rate of $CH_4$ at 200 mL $min^{-1}$ [standard temperature and pressure, STP]. The effluent gases from the bottom of the reactor were introduced into a Varian 3800 gas chromatograph for on-line gas compositional analysis, which was equipped with a Hayesep Q, a Poraplot Q, a 5 Å sieve molecular capillary column and a thermal conductivity detector (TCD) for the

separation and detection of $H_2$, $O_2$, CO, $CO_2$ and $CH_4$. The catalytic reactions were performed at 600–800 °C. The conversions of $CH_4$ ($C_{CH_4}$) and $O_2$ ($C_{O_2}$) and the selectivity of CO ($S_{CO}$) and $CO_2$ ($S_{CO_2}$) were calculated according to eqn (1), (2), (3) and (4), respectively.

$$C_{CH_4}(\%) = \frac{[CO] + [CO_2]}{[CO] + [CO_2] + [CO_4]_{outlet}} \times 100\% \quad (1)$$

$$C_{O_2}(\%) = \frac{0.5[CO] + [CO_2] + 0.5[H_2O]}{0.5[CO] + [CO_2] + 0.5[H_2O] + [O_2]_{outlet}} \times 100\% \quad (2)$$

$$S_{CO}(\%) = \frac{[CO]}{[CO] + [CO_2]} \times 100\% \quad (3)$$

$$S_{CO_2}(\%) = \frac{[CO_2]}{[CO] + [CO_2]} \times 100\% \quad (4)$$

### Electrochemical test

The area specific resistance (ASR) of the cathode materials was obtained by electrochemical impedance spectra (EIS) measurement using a Solartron 1287 potentiostat/galvanostat in combination with a Solartron 1260A frequency response analyser. The frequency range of the EIS measurement was from 100 kHz to 0.1 Hz with the signal amplitude of 10 mV. The cathode materials with a thin layer of silver as current collectors were tested under open circuit voltage (OCV) condition in air.

For the single cell test, the as-fabricated symmetrical SOFC was sealed onto a quartz tube with a silver paste (DAD-87, Shanghai, China). Hydrogen (80 mL $min^{-1}$ [STP]) or the $CH_4$–$O_2$ gas mixture ($CH_4$: 100 mL $min^{-1}$ [STP], $O_2$: 50 mL $min^{-1}$ [STP]) was fuelled into the anode side, while the cathode side was exposed to ambient air. The *I–V* polarization was measured for assessing the cell performance using a Keithley 2420 source meter. The impedance of a single cell under the OCV condition was also tested.

## Results and discussion

### Basic properties

LCFN was proven to have a high electrical conductivity and good and comparable electrochemical activity for ORR to the typical mixed conducting $La_{0.6}Sr_{0.4}Co_{0.2}Fe_{0.8}O_{3-\delta}$ (LSCF) perovskite electrode at elevated temperature, but cheaper raw materials.[20–23] In this study, LCFN was selected as the main component of the electrodes for the "symmetrical" SOFCs. The XRD patterns of LCFN, SDC, LCFN-infiltrated SDC (calcined at 800 °C in air) and the calcined LCFN-infiltrated SDC after the treatment at 700 °C in 10% $H_2$–Ar atmosphere for 10 h and 95 h are presented in Fig. 1. LCFN was reported to have an orthorhombic perovskite lattice structure with the space group *Pnma*, similar to those of $LaFeO_3$ and $La_{0.6}Ca_{0.4}FeO_{3-\delta}$.[24,25] All the diffraction peaks of the as-synthesized LCFN after the calcination at 1000 °C can be well indexed based on the orthorhombic perovskite structure, suggesting the successful formation of a single phase LCFN. For the XRD pattern of the LCFN-infiltrated SDC after calcination at 800 °C for 2 h in air, all the diffraction peaks can be indexed perfectly based on a physical mixture of a perovskite phase and a fluorite phase. The lattice parameters for both phases were determined based on the Rietveld refinement, and they turned out to be $a = 5.48(7)$ Å, $b = 7.75(3)$ Å, $c = 5.51(3)$ Å for the perovskite phase and $a = b = c = 5.433(5)$ Å for the fluorite phase, which matched pretty well with that of the LCFN and SDC phases, respectively.[22,26] It suggests the reaction between LCFN and the porous SDC scaffold was negligible at 800 °C. After the treatment in 10% $H_2$–Ar atmosphere at 700 °C for 10 h, or longer (95 h), the diffraction pattern of the sample still resembled that of the fresh one, which were well indexed based on a perovskite phase ($a = 5.52(2)$ Å, $b = 7.80(2)$ Å, $c = 5.55(5)$ Å) and a fluorite phase ($a = b = c = 5.435(5)$ Å). It suggests the main perovskite structure survived after the treatment in the reducing atmosphere. As compared to that of the fresh sample, the peak positions of the fluorite phase almost did not change for the sample after the treatment while the peaks for the perovskite phase shifted to a lower angle, indicating the expansion of the perovskite lattice. It suggests certain cation(s) in the perovskite phase was/were likely to be partially reduced. Nevertheless, the successful survival of the main perovskite phase under the reducing atmosphere could minimize internal strain during cell operation, thus benefiting the cell operation stability.

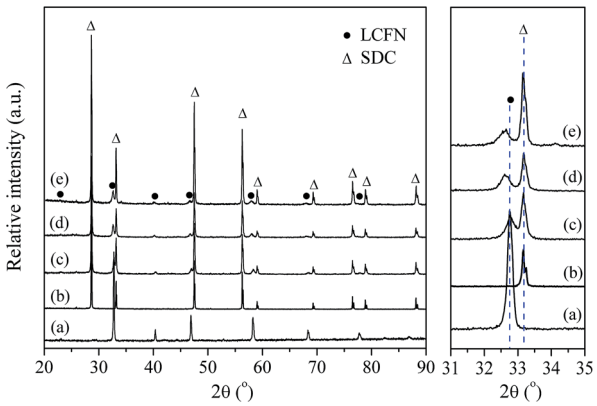


Fig. 1 XRD patterns of (a) LCFN, (b) SDC, (c) LCFN-infiltrated SDC after calcination in air at 800 °C and (d) calcined LCFN-infiltrated SDC after further treatment at 700 °C in 10% $H_2$–Ar atmosphere for 10 h and (e) 95 h.

The expanded perovskite lattice of LCFN after the treatment in 10% $H_2$–Ar atmosphere was further supported by the HR-TEM observation. As shown in Fig. 2, for the fresh LCFN-infiltrated SDC (Fig. 2a), diffraction fringes with the distance of 0.263 nm were observed, which matched well to the fringe distance of the [200] plane of the LCFN perovskite phase. Regarding the LCFN-infiltrated SDC after the treatment in 10% $H_2$–Ar atmosphere (Fig. 2b), similar fringes were detected for selected particles, but the fringe distance slightly increased to 0.267 nm. It further supports the fact that the lattice parameter slightly increased for the LCFN perovskite phase after the treatment under the reducing atmosphere.

 

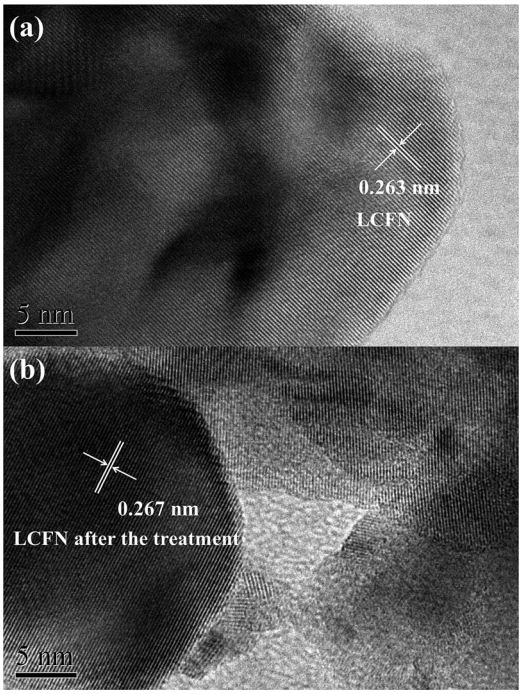


Fig. 2 HR-TEM images of (a) LCFN-infiltrated SDC after calcination in air at 800 °C and (b) calcined LCFN-infiltrated SDC after further treatment at 700 °C in 10% $H_2$–Ar atmosphere for 10 h.

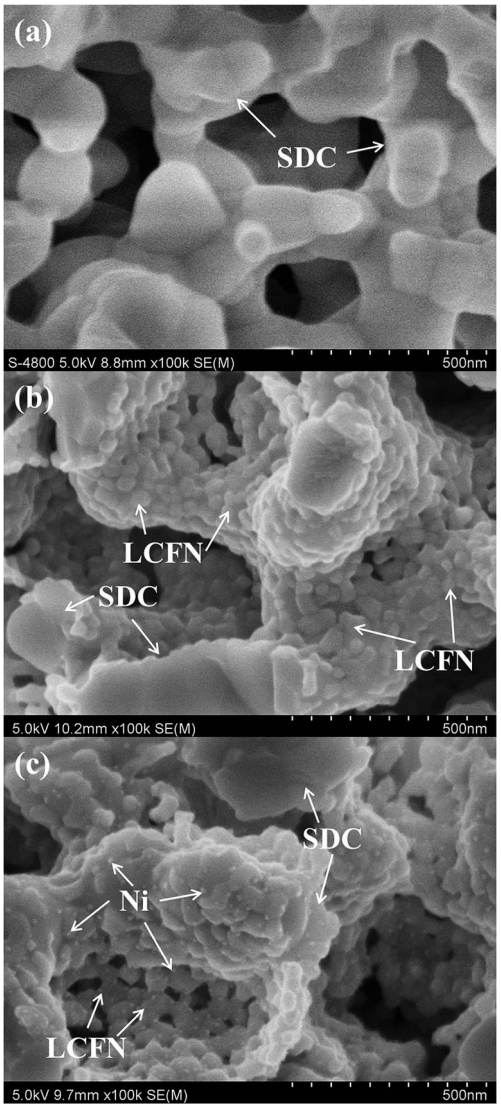


Fig. 3 SEM images of (a) porous SDC scaffold, (b) LCFN-infiltrated SDC after calcination in air at 800 °C and (c) calcined LCFN-infiltrated SDC after further treatment in 10% $H_2$–Ar at 700 °C for 10 h.

Fig. 3 presents the SEM images of the porous SDC scaffold (Fig. 3a), the LCFN-infiltrated SDC composite after the calcination in air at 800 °C (Fig. 3b) and the calcined LCFN-infiltrated SDC composite after further treatment in 10% $H_2$–Ar at 700 °C for 10 h (Fig. 3c). For the SDC scaffold, the SDC grains with the size of 0.2–0.4 μm with a polygonal shape were well sintered to form a continuous network with a porous architecture. After the infiltration with LCFN and calcination at 800 °C, the inner walls of the porous SDC scaffold were heavily decorated with spherical LCFN nanoparticles with a homogeneous particle size of around 80 nm. Such nanoparticles were well connected to form a continuous network, which may significantly increase the electrical conductivity of the electrode for the high conductivity of the LCFN phase. The calcined LCFN-infiltrated SDC was then subjected to further treatment under the reducing atmosphere. The overall electrode microstructure did not change significantly after the treatment. It further supported the fact that the main perovskite structure did not collapse under the reducing atmosphere. The main difference in morphology to that of the untreated electrode is that a lot of spherical shaped small particles with a size of approximately 10 nm appeared, which was distributed homogeneously over the surface of the LCFN nanoparticles. It suggests that some element possibly segregated from the perovskite phase as nanoparticles to decorate the perovskite oxide surface. Previously, it was demonstrated that some elements could be segregated from the perovskite oxide lattice as nanoparticles in the metallic phase to decorate the surface of the main perovskite oxide by chemical or electrochemical reduction.[27,28] Due to the higher reducibility of nickel cation compared to iron cation, it was likely that the formed nanoparticles were the metallic nickel phase.

To further analyse the composition of the electrode after the treatment in the $H_2$ atmosphere, it was subjected for STEM analysis with the image shown in Fig. 4. The STEM image clearly shows that the large SDC grains were surrounded by smaller particles. The EDX analysis of the surrounding particles demonstrated the compositions of La, Ca, Fe and Ni, indicating the successful impregnation of the LCFN phase into the SDC scaffold. As compared to the other elements, nickel showed a less homogeneous distribution than the other elements. It implies that nickel was extracted from the perovskite lattice under reducing atmosphere.

To ensure a high operational stability of an SOFC, the cell components should have good thermo-mechanical compatibility. The mismatch in TECs between the electrode and electrolyte layers could create large internal strain during the

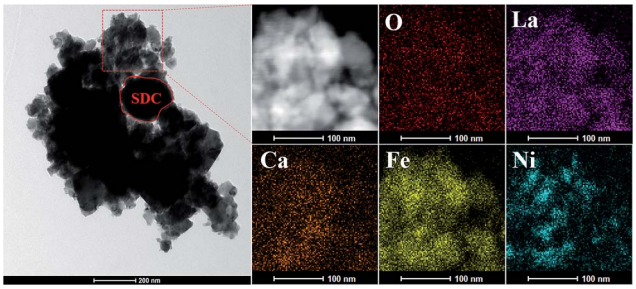


Fig. 4 STEM image and EDX elemental distribution of La, Ca, Fe, Ni and O in the LCFN-infiltrated SDC electrode after the treatment in 10% $H_2$–Ar at 700 °C for 10 h.

heating and cooling processes, which could induce the delamination of the electrode from electrolyte layer, a main cause of the degradation in cell performance. Fig. 5 shows the thermal expansion curves of the pure LCFN and LCFN-infiltrated SDC samples under different atmospheres. For the pure LCFN in air, the average TEC in the temperature range of 200–900 °C was calculated to be 23.0 $\times$ $10^{-6}$ $K^{-1}$ according to the $d\Delta L/L_0$ *vs.* temperature curve, and the TEC even reached higher than 38.4 $\times$ $10^{-6}$ $K^{-1}$ at around 550 °C (Fig. 5a). As for the LCFN-infiltrated SDC composite at the same atmosphere, the average TEC was 11.5 $\times$ $10^{-6}$ $K^{-1}$ between 200 and 900 °C (Fig. 5b), which was comparable to that of pure SDC (a TEC of 12.3 $\times$ $10^{-6}$ $K^{-1}$ was reported),[29] agreeing well with the fact that the TEC of the infiltrated electrode was mainly determined by the porous scaffold.[30] Under the reducing atmosphere, the average TEC of the LCFN-infiltrated SDC was 16.4 $\times$ $10^{-6}$ $K^{-1}$, which was a little bit higher than that of the sample tested in air. It is probable that partial nickel reduced from the LCFN-infiltrated SDC, affected the TEC. However, the TEC of 16.4 $\times$ $10^{-6}$ $K^{-1}$ for the reduced LCFN-infiltrated SDC was still comparable to that of SDC. The similar TECs of the LCFN-infiltrated SDC to SDC provided good thermo-mechanical compatibility between the electrodes and electrolyte, ensuring a better operational stability in the real SOFC.

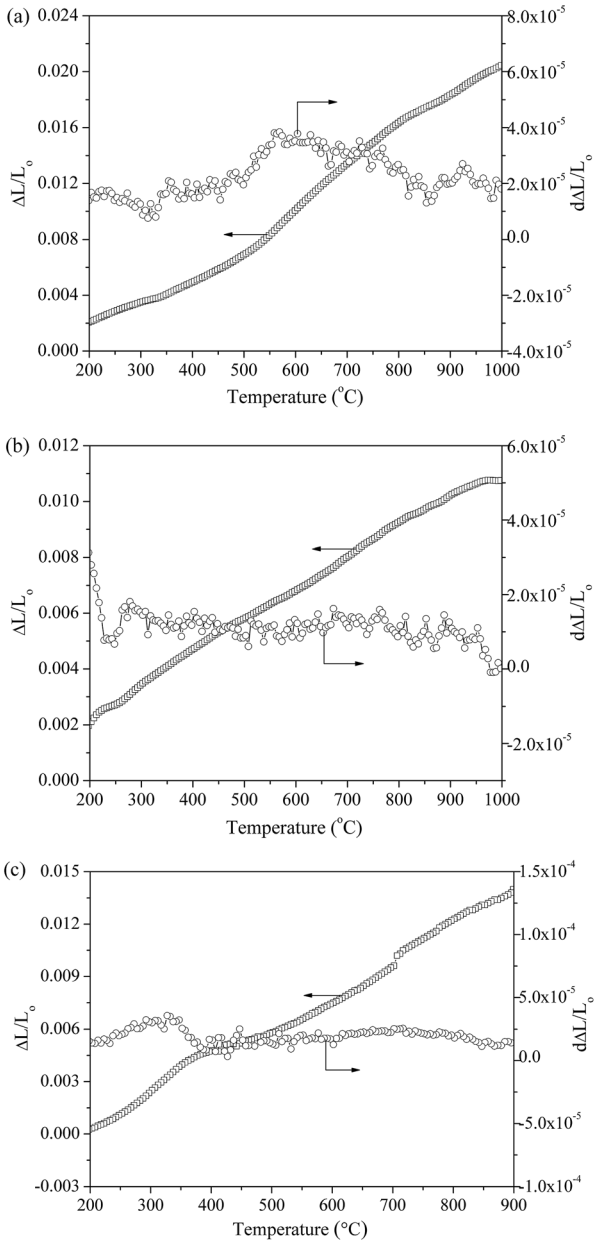


Fig. 5 The thermal expansion curves of (a) pure LCFN and (b) LCFN-infiltrated SDC in air, and (c) LCFN-infiltrated SDC under 10% $H_2$–Ar atmosphere.

### Electrocatalytic activity for ORR

In literature, a single phase LCFN was typically used as the cathode of SOFCs.[20–23] It is well known that the electrochemical performance of a cathode is also highly dependent on the electrolyte that gets deposited on it.[22,31] In this study, the ASRs of the LCFN-infiltrated SDC electrode on the SDC electrolyte in an air atmosphere were measured based on the symmetrical configuration with the typical EIS curves at 600 °C shown in Fig. 6, while the ASRs of electrode at various temperatures are listed in Table 1. For comparison, the ASRs of the single phase LCFN electrode and a conventional LCFN–SDC composite electrode (weight ratio of LCFN to SDC is 30 : 70) prepared by physical mixing method were also measured and presented.

By applying the single phase LCFN as the electrode, ASRs of 11.70, 2.93, 0.89, 0.32 and 0.14 Ω $cm^2$ were achieved at 550, 600, 650, 700 and 750 °C, respectively, which were much smaller than the reported ASR of the LCFN electrode on the YSZ electrolyte, for example, 85.87 Ω $cm^2$ even at 850 °C.[20] It further supported the fact that the electrolyte had an impact on the electrochemical performance of the electrode material. For the conventional physically mixed LCFN–SDC composite electrode, ASRs of 6.72, 2.54, 1.20, 0.65 and 0.37 Ω $cm^2$ were obtained at 550, 600, 650, 700 and 750 °C, respectively, which are modestly better than that of the single phase LCFN electrode. Such improvement may be explained by the increased apparent oxygen-ion conductivity of the electrode from the incorporation of the SDC phase, resulting in increased electrochemically active sites for ORR. For the nano LCFN-infiltrated SDC electrode, ASRs of 0.36, 0.12, 0.053, 0.021 and 0.009 Ω $cm^2$ were

 

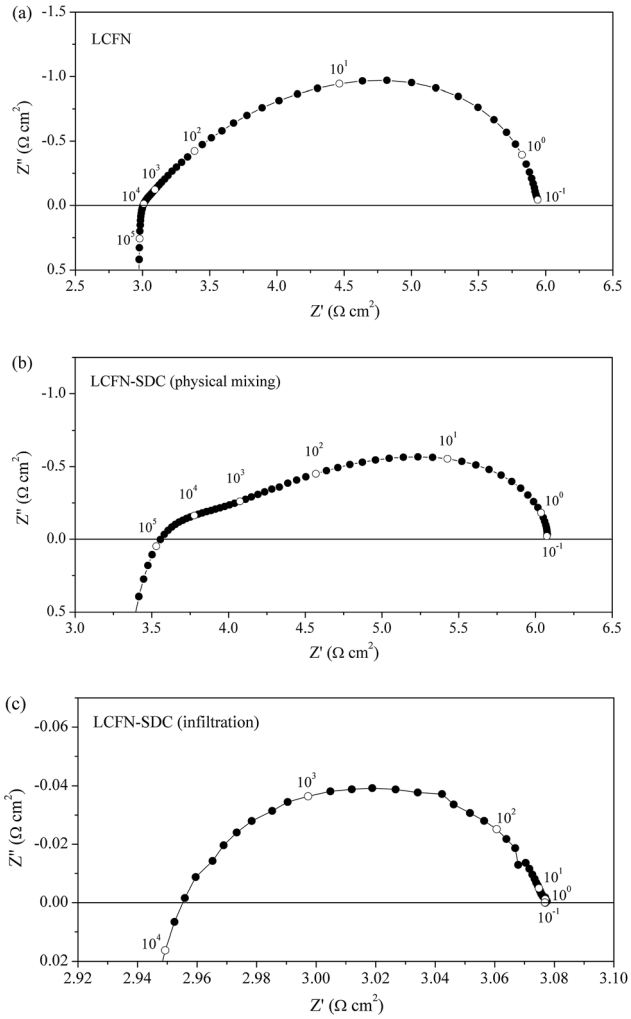


Fig. 6 The Nyquist impedance curves for the symmetrical cells with (a) pure LCFN, (b) LCFN–SDC (physical mixing) and (c) LCFN-infiltrated SDC electrodes on the SDC electrolyte measured at 600 °C in air.

Table 1 ASRs of LCFN, LCFN–SDC electrode prepared by physical mixing (LCFN–$SDC_p$) and LCFN-infiltrated SDC electrode (LCFN–$SDC_i$) on the SDC electrolyte measured between 550 and 750 °C

| | ASR (Ω $cm^2$) | | | | |
|---|---|---|---|---|---|
| Electrode | 550 °C | 600 °C | 650 °C | 700 °C | 750 °C |
| LCFN | 11.70 | 2.93 | 0.89 | 0.32 | 0.14 |
| LCFN–$SDC_p$ | 6.72 | 2.54 | 1.20 | 0.65 | 0.37 |
| LCFN–$SDC_i$ | 0.36 | 0.12 | 0.053 | 0.021 | 0.0091 |

achieved at 550, 600, 650, 700 and 750 °C, respectively. It indicates that the infiltrated LCFN–SDC composite electrode had the best electrochemical performance for ORR among the various LCFN-based electrodes. Such improvement can be explained by the specific electrode architecture, which provided the optimal charge transfer path. The continuous SDC scaffold provided a fast oxygen ion diffusion path to the electrolyte, while LCFN had much higher surface exchange kinetics than SDC, thus the decoration of the SDC surface with LCFN effectively improved the activity for surface oxygen dissociation and surface diffusion, thus successfully improving the overall surface kinetics. In addition, it was reported that the smaller electrode particle size benefits the ORR process,[32] hence, the nano LCFN particle as obtained by the infiltration process also contributed to the outstanding performance of the current LCFN–SDC.

## Activity for methane oxidation

It was reported that the $La_{1-x}Ca_xFeO_{3-\delta}$ perovskite oxide has high catalytic activity for methane combustion,[33] while nickel is a good catalyst for methane partial oxidation and electrocatalytic oxidation of $H_2$ to $H_2O$.[6] By applying methane as a fuel, the indirect electro-catalytic oxidation pathway, *i.e.*, the first internal reforming of methane to hydrogen, and then the electro-oxidation of hydrogen to generate electricity is easier to achieve a higher power output than the direct electro-oxidation of methane since the electrochemical oxidation rate of hydrogen is much faster than methane over conventional anode catalysts.

To get information about the activity of the LCFN–SDC composite as an anode, the catalytic activity of fresh and reduced LCFN powders for methane oxidation were tested respectively with a stream of the $CH_4$–$O_2$ gas mixture at a molar ratio of 2 : 1 as the reactants. As shown in Fig. 7, an affordable methane and oxygen conversion was obtained when the fresh LCFN was applied as the catalyst. For example, at 600 °C methane and oxygen conversions reached 12.5% and 63.5%, respectively. The LCFN catalyst mainly showed activity for the methane deep oxidation at 600 °C, as indicated by $CO_2$ which was the main carbon-containing product, while the CO content in the effluent gas was fairly low. It agrees well with the fact that perovskite oxides are usually active for the deep oxidation of hydrocarbons.[34] As for the LCFN catalyst after the treatment in the 10% $H_2$–Ar reducing atmosphere, the methane conversion was 26.5% at 600 °C and the oxygen conversion even reached 100% at 600 °C, suggesting the improved activity after the treatment. With the increase of the operation temperature, an increase in CO selectivity was observed for both the fresh and treated LCFN catalysts; however the treated catalyst always showed higher methane conversion and CO selectivity than the fresh LCFN catalyst. It agrees well with the fact that some metallic nickel was segregated after the reduction as demonstrated in the previous study. It is well known that nickel is a highly active catalyst for methane partial oxidation and $CO_2$/steam reforming. Since hydrogen has a much higher electro-oxidation rate than methane while nickel has much a higher electrocatalytic activity than perovskite oxides, it suggests that the segregation of nickel from the perovskite lattice would also make LCFN a good anode candidate.

## "Symmetrical" SOFC performance

Based on the above analysis, LCFN could be a good candidate for both the anode and the cathode of SOFCs. An SDC electrolyte-supported "symmetrical" SOFC with a nano LCFN-

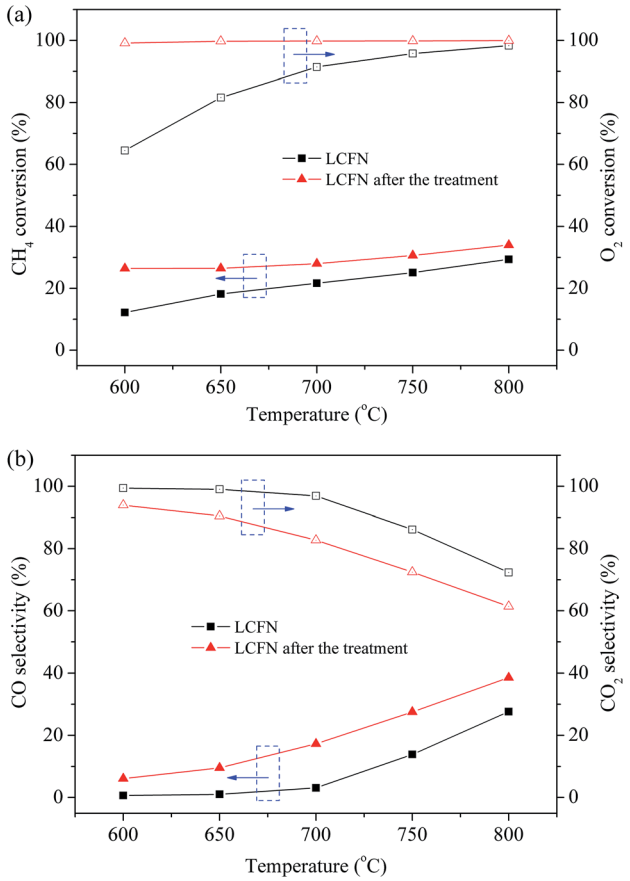


Fig. 7 The catalytic activity of fresh LCFN and LCFN after the treatment in 10% $H_2$–Ar at 700 °C for 10 h for methane oxidation ($CH_4$ : $O_2$ = 2 : 1) between 600 and 800 °C: (a) $CH_4$ and $O_2$ conversions, (b) $CO_2$ and CO selectivity.

infiltrated porous SDC scaffold as the electrodes was then fabricated and tested. The electrolyte and electrodes had a thickness of around 300 and 20 μm, respectively. The cell was first subjected for operation on hydrogen fuel. As shown in Fig. 8, OCVs of 0.9–0.8 V were obtained between 600 and 800 °C, and steadily decreased with the operation temperature increased. The relatively low OCV can be explained by the partial electronic conductivity of SDC at temperatures higher than 600 °C. Anyway, the OCVs were in well agreement with the literature results for a cell with an SDC electrolyte and Ni–SDC anode.[35] It suggests that the nano LCFN decorated SDC electrode performed soundly as an anode for SOFCs. The near linear response of the cell voltage to the polarization current at different temperatures, even at a high current density, indicates that the electrodes were sufficiently porous to avoid concentration polarization even at high temperatures and large polarization current density conditions. Peak power densities (PPDs) of 196, 276, 362, 444 and 507 mW $cm^2$ were achieved at 600, 650, 700, 750 and 800 °C, respectively. Such results are highly attractive when considering large thickness of the electrolyte membrane (0.3 mm).

To get information about the contribution of resistance from the different cell components, the impedance of the cell under OCV conditions was also measured and the typical spectra are shown in Fig. 9. Although the impedance of the single cell was fairly complicated, the intercept of the impedance arc at the low frequency side with the real axis usually embodies the overall cell resistance ($R$) while the intercept of the impedance arc at the high frequency section with the real axis represents the cell ohmic resistance ($R_o$). The difference between two intercepts is a sum of the polarization resistance ($R_p$) from both the anode and cathode. From Fig. 9, it is clear that the main cell resistance was contributed from the electrolyte ohmic resistance ($R_o$), in particular at higher temperatures. Table 2 lists the ohmic (or polarization) resistances of the electrolyte and electrode, and the overall percentage of the electrolyte resistance to the total resistance at different temperatures. The electrolyte ohmic resistance ($R_o$) accounted for 95.3% of the total cell resistance at 800 °C, while it still accounted for 82.9% at 600 °C. Thus, an obvious improvement in cell performance is expected if the electrolyte thickness could be further reduced, or the adoption of an alternative electrolyte material with higher conductivity, such as the newly discovered superior oxide-ion conductor $Sr_{3-3x}Na_{3x}Si_3O_{9-1.5x}$ ($x = 0.45$).[36]

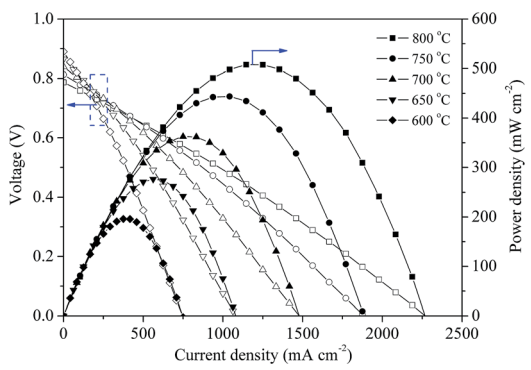


Fig. 8 $I$–$V$ and $I$–$P$ curves of the cell with the configuration of LCFN-infiltrated SDC|SDC|LCFN-infiltrated SDC operating on hydrogen.

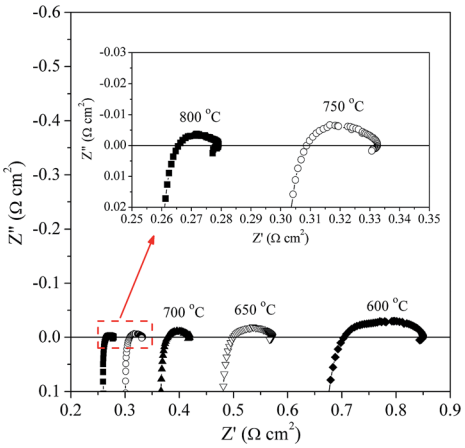


Fig. 9 The impedance spectra of the cell (LCFN-infiltrated SDC|SDC|LCFN-infiltrated SDC) operating on hydrogen at different temperatures under OCV conditions.

Table 2 The resistances of the electrolyte ($R_o$) and electrode ($R_p$), and the overall percentage of electrolyte resistance to the total resistance at different temperatures

| Temperature (°C) | $R_o$ (Ω cm$^2$) | $R_p$ (Ω cm$^2$) | $R_o/(R_o + R_p)$ |
|---|---|---|---|
| 800 | 0.266 | 0.013 | 95.3 |
| 750 | 0.309 | 0.024 | 92.8 |
| 700 | 0.379 | 0.045 | 89.4 |
| 650 | 0.500 | 0.072 | 87.4 |
| 600 | 0.705 | 0.145 | 82.9 |

As was demonstrated previously, the reduced LCFN electrode showed improved activity for the methane deep oxidation and reforming reaction. It implies that the nano LCFN-infiltrated SDC electrode could also perform well for the operation on a methane-based fuel. Hence, the "symmetrical" SOFC was then tested using the gas mixture of methane–oxygen as the fuel. As shown in Fig. 10, PPDs of 160, 220, 280 and 350 mW cm$^{-2}$ was achieved at 650, 700, 750 and 800 °C, respectively. Although the results were a little worse than that the operation on hydrogen, they are still highly attractive by considering the symmetrical cell and thick electrolyte membrane configuration, and methane as the direct fuel without pre-reforming.

After the fuel cell test under various conditions ($H_2$ and $CH_4$–$O_2$ fuels, 600–800 °C and different polarization currents), the cell was cooled down to room temperature for SEM observation. As shown in Fig. 11, the electrodes still adhered to the electrolyte surfaces without the appearance of any delamination. After the operation, the nano-size particulate morphology of LCFN in the cathode was still well maintained, and the LCFN particle size was maintained at approximately 80 nm (inset of Fig. 11a), similar to that of LCFN in the freshly prepared electrode. It suggests such nano LCFN-infiltrated electrode can be stably operated under cathode conditions. As to the infiltrated LCFN electrode operated under anode conditions, as shown in the inset of Fig. 11b, the electrode microstructure was also well maintained, and the nickel particles were still distributed over the surface of LCFN nanoparticles homogeneously. Noteworthy, the nickel nanoparticles became somewhat larger in size after the operation, which suggested sintering. However, due to the special symmetrical configuration, by switching the anode and cathode roles, the potential degradation due to nickel sintering can be easily recovered through the electrode regeneration.[37]

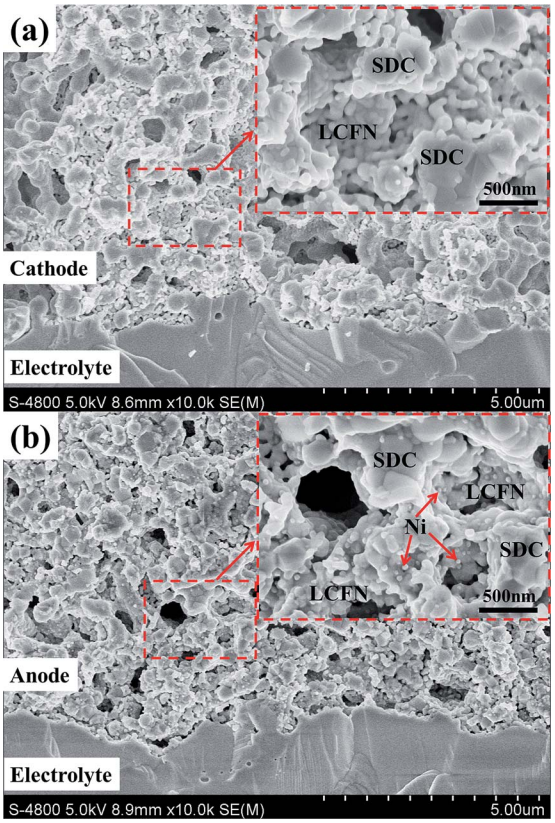


Fig. 11 SEM images of (a) cathode–electrolyte and (b) anode–electrolyte interfaces. Inset: the magnification of cathode and anode.

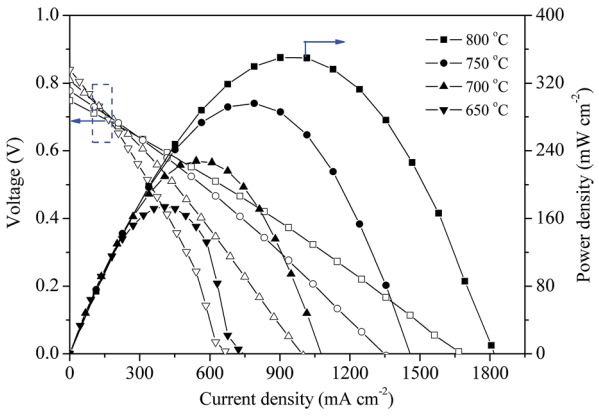


Fig. 10 $I$–$V$ and $I$–$P$ curves of the cell with the configuration of LCFN-infiltrated SDC|SDC|LCFN-infiltrated SDC operating on a $CH_4$–$O_2$ gas mixture at the molar ratio of 2 : 1.

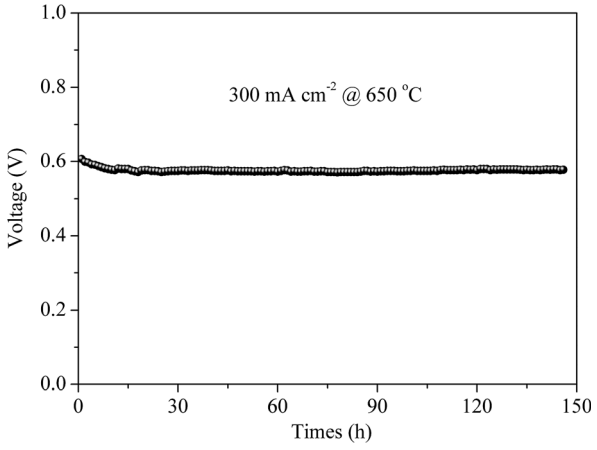


Fig. 12 Time dependence of the cell voltage with 3% $H_2O$ humidified $H_2$ fuel under a constant polarization current of 300 mA cm$^{-2}$ at 650 °C.

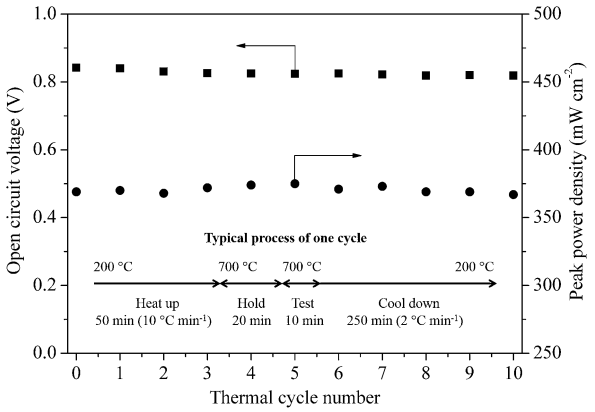


Fig. 13 The thermal cycling stability of the symmetrical SOFC with the LCFN-infiltrated SDC electrode.

The operation stability is a significant concern for the practical application of SOFCs. Fig. 12 shows the operation stability of the SDC electrolyte-supported SOFC with symmetrical LCFN-infiltrated SDC electrodes using 3% $H_2O$ humidified $H_2$ as the fuel under a constant polarization current density of 300 mA cm$^{-2}$ at 650 °C. The cell voltage was maintained at around 0.58 V for a period over 140 h, indicating that the LCFN-infiltrated SDC electrode could be stably operated under both anode and cathode conditions.

Finally, the thermal cycling test was conducted to investigate the thermo-mechanical stability of the "symmetrical" SOFC with LCFN-infiltrated SDC electrode. The cell was heated up and cooled down between 200 and 700 °C ten times. As shown in Fig. 13, the thermal cycling process has little effect on the cell performance, for example, the OCV and PPD of the cell kept at around 0.82 V and 370 mW cm$^{-2}$ during the 10 cycling tests, indicating that the symmetrical cell with the LCFN–SDC electrode possesses excellent thermo-mechanical stability.

## Conclusions

We have demonstrated that the nano LCFN-infiltrated porous SDC composite is a promising electrode material for both the anode and cathode of "symmetrical" SOFCs due to both the excellent anode and cathode performance. As for the anode, the nickel particles in the LCFN oxide were partially segregated from the perovskite lattice that decorated the surface of LCFN under the reducing atmosphere, thus delivering the high catalytic activity for the chemical and electrochemical oxidation of fuels. The main perovskite structure of LCFN did not change which ensured the good mechanic-chemical compatibility of the cell components. As for the cathode, the LCFN-infiltrated SDC electrode exhibited excellent ORR activity with an ASR of 0.12 Ω cm$^2$ at 600 °C in air. The peak power densities of the thick electrolyte-supported SOFC with the LCFN–SDC electrode reached 510 and 350 mW cm$^{-2}$ at 800 °C operating on hydrogen and $CH_4$–$O_2$ fuels, respectively, which are highly attractive when considering the use of a thick electrolyte. The electrode microstructure was hardly changed after the fuel cell test under various conditions. The cell was operated stably for over 140 h. The good thermo-mechanical stability of the cell was also demonstrated. Our study opens up a new avenue for promoting the practical application of the SOFC technology.

## Acknowledgements

The authors acknowledge the support from the Australian Research Council Future Fellowship under the contract of FT100100134.

## Notes and references

1 B. C. H. Steele and A. Heinzel, *Nature*, 2001, **414**, 345.
2 K. Y. Chan, J. Ding, J. W. Ren, S. A. Cheng and K. Y. Tsang, *J. Mater. Chem.*, 2004, **14**, 505.
3 Z. P. Shao and S. M. Haile, *Nature*, 2004, **431**, 170.
4 M. D. Gross, J. M. Vohs and R. J. Gorte, *J. Mater. Chem.*, 2007, **17**, 3071.
5 D. J. Chen, G. M. Yang, F. Ciucci, M. O. Tadé and Z. P. Shao, *J. Mater. Chem. A*, 2014, **2**, 1284.
6 W. Wang, C. Su, Y. Z. Wu, R. Ran and Z. P. Shao, *Chem. Rev.*, 2013, **113**, 8104.
7 F. F. Dong, D. J. Chen, Y. B. Chen, Q. Zhao and Z. P. Shao, *J. Mater. Chem.*, 2012, **22**, 15071.
8 J. B. Goodenough and Y. H. Huang, *J. Power Sources*, 2007, **173**, 1.
9 A. Lashtabeg and S. J. Skinner, *J. Mater. Chem.*, 2006, **16**, 3161.
10 D. M. Bastidas, S. W. Tao and J. T. S. Irvine, *J. Mater. Chem.*, 2006, **16**, 1603.
11 J. C. Ruiz-Morales, D. Marrero-Lopez, J. Canales-Vazquez and J. T. S. Irvine, *RSC Adv.*, 2011, **1**, 1403.
12 T. Wei, Q. Zhang, Y. H. Huang and J. B. Goodenough, *J. Mater. Chem.*, 2012, **22**, 2251.
13 Y. Lin, C. Su, C. Huang, J. S. Kim, C. Kwak and Z. P. Shao, *J. Power Sources*, 2012, **197**, 57.
14 Q. Liu, X. H. Dong, G. L. Xiao, F. Zhao and F. L. Chen, *Adv. Mater.*, 2010, **22**, 5478.
15 B. Lin, S. L. Wang, X. Liu and G. Y. Meng, *J. Alloys Compd.*, 2010, **490**, 214.
16 S. W. Tao and J. T. S. Irvine, *Nat. Mater.*, 2003, **2**, 320.
17 J. C. Ruiz-Morales, J. Canales-Vázquez, B. Ballesteros-Pérez, J. Peña-Martínez, D. Marrero-López, J. T. S. Irvine and P. Núñez, *J. Eur. Ceram. Soc.*, 2007, **27**, 4223.
18 G. M. Yang, C. Su, R. Ran, M. O. Tadé and Z. P. Shao, *Energy Fuels*, 2013, **28**, 356.
19 D. J. Chen, R. Ran and Z. P. Shao, *J. Power Sources*, 2010, **195**, 4667.
20 I. Ruiz de Larramendi, N. Ortiz, J. I. Ruiz de Larramendi and T. Rojo, *ECS Trans.*, 2007, **7**, 1157.
21 N. Ortiz-Vitoriano, A. Hauch, I. Ruiz de Larramendi, C. Bernuy-Lopez, R. Knibbe and T. Rojo, *J. Power Sources*, 2013, **239**, 196.
22 N. Ortiz-Vitoriano, I. Ruiz de Larramendi, I. G. de Muro, J. I. Ruiz de Larramendi and T. Rojo, *Mate. Res. Bull.*, 2010, **45**, 1513.

 

23 N. Ortiz-Vitoriano, I. Ruiz de Larramendi, S. N. Cook, M. Burriel, A. Aguadero, J. A. Kilner and T. Rojo, *Adv. Funct. Mater.*, 2013, **23**, 5131.
24 M. Palcut, J. S. Christensen, K. Wiik and T. Grande, *Phys. Chem. Chem. Phys.*, 2008, **10**, 6544.
25 J. M. Hudspeth, G. A. Stewart, A. J. Studer and D. J. Goossens, *J. Phys. Chem. Solids*, 2011, **72**, 1543.
26 T. Skalar, J. Maček and A. Golobič, *J. Eur. Ceram. Soc.*, 2012, **32**, 2333.
27 G. Tsekouras, D. Neagu and J. T. S. Irvine, *Energy Environ. Sci.*, 2013, **6**, 256.
28 S. H. Cui, J. H. Li, X. W. Zhou, G. Y. Wang, J. L. Luo, K. T. Chuang and L. J. Qiao, *J. Mater. Chem. A*, 2013, **1**, 9689.
29 E. Y. Pikalova, V. I. Maragou, A. N. Demina, A. K. Demin and P. E. Tsiakaras, *J. Power Sources*, 2008, **181**, 199.
30 F. C. Wang, D. J. Chen and Z. P. Shao, *J. Power Sources*, 2012, **216**, 208.
31 F. F. Dong, D. J. Chen, R. Ran, H. J. Park, C. Kwak and Z. P. Shao, *Int. J. Hydrogen Energy*, 2012, **37**, 4377.
32 Z. Y. Jiang, C. R. Xia and F. L. Chen, *Electrochim. Acta*, 2010, **55**, 3595.
33 P. Ciambelli, S. Cimino, L. Lisi, M. Faticanti, G. Minelli, I. Pettiti and P. Porta, *Appl. Catal., B*, 2001, **33**, 193.
34 J. G. McCarty and H. Wise, *Catal. Today*, 1990, **8**, 231.
35 W. Zhou, Z. P. Shao, R. Ran, W. Q. Jin and N. P. Xu, *Chem. Commun.*, 2008, **44**, 5791.
36 T. Wei, P. Singh, Y. H. Gong, J. B. Goodenough, Y. H. Huang and K. Huang, *Energy Environ. Sci.*, 2014, **7**, 1680.
37 S. S. Li, Q. Q. Qin, K. Xie, Y. Wang and Y. C. Wu, *J. Mater. Chem. A*, 2013, **1**, 8984.